International Symposium of Research Students on Materials Science and Engineering
December 20-22, 2004, Chennai, India
Department of Metallurgical and Materials Engineering, Indian Institute of Technology Madras

DEGRADATION OF MATERIAL PROPERTIES OF A CUPRONICKEL ALLOY IN AMMONIACAL ENVIRONMENTS

Commander DC Agarwal, Indian Navy and Commandant (JG) Alankar Singh Indian Coast Guard

ABSTRACT

The present author(s) have studied several marine environment field failures of bent and branched copper-nickel pipelines exposed to marine environments with ammoniacal byproduct. The cause of failures was examined through laboratory test on a 5.37% Cu-Ni alloy, used in the failed pipes, and tests were conducted under Slow Strain Rate Test (SSRT) conditions, in aqueous ammonia and ammoniacal seawater environments. These studies revealed that the presence of ammonia in seawater impairs the load bearing capacity of the alloy, and the aqueous ammonia environments tend to cause brittle Stress Corrosion Cracking (SCC) type failures, which are often premature and/or catastrophic. However, in addition to induced residual stresses from manufacturing/ processing, the operating conditions in marine environments subject these pipes to external forces and widely varying pressures and fluid flow rates, which can cause both static and cyclic stresses. A static load with fixed-interval, low-amplitude cyclic loading conditions. Tests conducted under superimposed cyclic stresses on pre-stressed specimens accelerated the stress corrosion failure mechanism of the alloy in ammoniacal environment.Further tests under SSRT were conducted by introducing Magnesium Chloride ($MgCl_2$) along with ammonia. Exposure to ammonia in presence of $MgCl_2$ was found to reduce the ammonia induced SCC and the extent of loss of ductility. This paper presents the observed degradation of the material properties of the alloy under the influence of ammonia and its possible mitigating mechanism.

1 INTRODUCTION

Environment-assisted cracking [1] often leads to premature, catastrophic failures at stresses well below the design specifications, if the operating conditions become more severe than the design conditions. Metals and alloys specially developed for withstanding large stresses fail prematurely in marine environments because of corrosion from the chlorinated seawater and other pollutants that are invariably present in and around marine piping systems. While microstructural inhomogeneities, residual stresses etc., can also contribute to the failures, the environment-assisted failures are almost always dominated by corrosion and/or some form of stress corrosion cracking (SCC), both of which can be material and environment specific [2]. The amount of corrosion involved in SCC is usually minimal.

The excellent corrosion, erosion, cavitation, SCC, corrosion fatigue and bio-fouling resistance of Cu-Ni alloys make them very valuable in many marine applications

including in ship and boat hulls, offshore platform claddings, desalination plants, heat exchange equipment, seawater and hydraulic pipelines of ships, plumbing, oil rigs and platforms, fish-farming cages, and seawater intake screens. Consequently, Cu-Ni materials have been studied extensively in marine environments. By nature, the marine environments are very variable, therefore all the findings of a specific study may not be directly applicable to each and every real-life situation involving a marine application.

Many studies have been carried out on the effect(s) of constituent ingradients of seawater on Cu-Ni alloys [3 – 5]. Studies conducted with 3.5% NaCl solutions, using constant extension strain rates at different currents and pH levels, suggested that a higher pH level increased the time to failure although no evidence of stress cracking was found[6]. However, the decrease in the pH levels increased the corrosion current for any applied anodic potential. Tests conducted on 90/10 and 70/30 Cu-Ni alloys indicated that in unpolluted sea water both the alloys displayed similar resistance to corrosion [7]. In general, pollutants lead to an increase in the corrosion rate. 70/30 Cu-Ni is more resistant to the adverse effects of various pollutants. However, ammonium chloride and sulphide, followed by ammonium sulphide were found to be corrosive to the 70/30 Cu-Ni. For the 90/10 Cu-Ni alloy, the main corrosive pollutants were sulphides, followed by urea and chlorine.

The low-nickel copper alloys have been of interest to users and researchers alike since 1938 [8]. The alloys containing 5 – 10 % Ni and 1- 2% iron (Fe) were found to be of particular interest, as they offered optimum resistance to seawater corrosion, when quenched from temperatures of 850 – 950 deg C. Several premature failures of bent and branched Cu-Ni pipelines were encountered on ships, more commonly near the WC's and mud boxes [9]. These failed pipes are subjected to widely varying fluid flow rates, and are exposed to environment containing high percentages of magnesium chloride with smaller amounts of ammonia. It was suspected that the observed failures could be caused by magnesium chloride and/or ammonia, by compromising the load-bearing capacity of the material. Compositional and micro-structural testing of the failed pipes revealed that these pipes were made from a Cu-Ni alloy containing 5.38% nickel and an annealed grain structure. In order to develop a better understanding of the observed failures, the author conducted slow strain-rate corrosion testing on a low-nickel (5.37% Ni) commercial copper alloy, with the grain structure similar to that of the failed pipe material. Tests were carried out at ambient temperature using slow strain rates (SSRT) in air, and in solutions containing 3.5 % NaCl + 10% $MgCl_2$ + with and without 1% ammonia [9]. The test results suggested that the presence of magnesium does not directly enhance the corrosion rate, but may contribute to the formation of magnesium chloride, which is acidic in nature, and may promote general corrosion, resulting in the thinning of the copper nickel alloys, especially in flowing water. In the presence of ammonia, the test failures were found to occur by a corrosion-assisted, brittle failure mechanism, but SCC was not involved.

In a subsequent study of the same Cu-Ni alloy conducted in 5.0% aqueous ammonia, and in an ammoniacal solution containing 5.0% ammonia + 10.0% $MgCl_2$ + 3.5% NaCl. The 5.0% aqueous ammonia failures were found to occur by a brittle transgranular SCC mode, however, the characteristic crack branching normally observed in SCC was not present [10]. The observed absence of the crack branching was attributed to the SSRT

and the accelerated corrosion in the presence of 5.0% ammonia, which can mask the incipient crack branching that usually occurs at the crack tips in SCC. In ammoniacal solution, the operative corrosion mechanism was a brittle, intergranular failure with the attack originating from the sample surfaces, similar to the earlier tests [9]. The absence of SCC in the presence of $MgCl_2$ + NaCl was intriguing and additional tests were designed to study this phenomenon.

The initial strain rate employed in the conducted tests [9,10] was $1.18 * 10^{-7}$ sec^{-1}, and the test duration ranged from 15 - 27 days. To obtain quicker results, further tests were planned to be conducted per ISO 7539-7 [11], which recommends an initial strain rate of 10^{-6} sec^{-1} for the determination of SCC in Cu and Cu-Ni alloys. In order to check the suitability of the faster strain rates for the present tests, two identical samples were tested in air and in a solution of 3.5%NaCl +10%$MgCl_2$ + 1%NH_3 (ammoniacal solution) [12] with the two initial strain rates, $1.18* 10^{-7}$ sec^{-1} and $9.98 * 10^{-7}$ $sec,^{-1}$ respectively. The results from these tests indicated that the comparative mechanical properties can be assessed in different environments at the strain rate of 10^{-6} sec^{-1}, and the higher strain rates are also suitable for assessing the succeptibility to SCC in a specific environment.

The results obtained earlier [9,10] suggested that the ammonia concentration might be one of the key factors in determining the modes and mechanisms of the failures observed in Cu-Ni pipes in marine environments. In the present investigation, the subject Cu-5.37% Ni alloy specimens were tested in aqueous ammonia containing 1.0, 2.5, 5.0, 10.0 and 12.5 % ammonia, respectively [14]. Identical specimens were also tested in air to obtain the base-line inert environment data, and to verify the compatibility of the present test results with the previous test results [9, 10 and 12]. Analysis by optical microscopy, SEM/EDX analysis, and SEM fractography was carried out and the operative failure modes and mechanisms in the tested specimens were identified [14]. The test procedure adopted and results are reproduced below along with further analysis.

2. EXPERIMENTAL

2.1 Material Specification, Specimen Preparation and Test Apparatus

A 3.0 mm thick hot-rolled, copper-nickel alloy plate was used for the preparation of the test specimens. The alloy material, specimen preparation technique, test procedures employed were identical to those in the previous investigations [9,10,12].

Alloy Composition (Wt. %):

Cu	Ni	Fe	Mn	Zn	Pb	Sn
92.8	5.37	1.03	0.61	0.07	0.01	<0.01

Mechanical properties:

YS = 204.2 MN/m²; UTS = 337.1 MN/m²; % Elongation = 32 (50 mm guage length). Hardness = 56 HRB.

Microstructure: Fine grain, equiaxed, randomly oriented grain structure with a grain size of ASTM 8.5.

Specimen Specification and Dimensions: ASTM/E-8 [13] with a width of 12.573 mm in the center, increasing to 12.7 mm over a distance of 28.575 mm on either side was used. The guage length was 50 mm. The test specimens were wire-cut in the direction of rolling, polished with 340, 400 and 600 grit SiC paper, and then lapped to give a mirror surface finish. The finished specimens were examined under a microscope at 20X magnification to ensure that there were no scratch marks perpendicular to the direction of loading. The specimens were then rinsed with AR grade alcohol and dried prior to testing.

Test Rig: A Monsanto Tensometer equipped with an automatic thermal plotter and time recorder was used to conduct the tests. The tensometer was modified to provide a controlled maximum cross-head speed of 0.0017998 cm/min, which could be varied down linearly to the lowest crosshead speed of 0.0000199987 cm/min [9].

Corrosion Chamber: A PTFE tube, with a slider arrangement and neoprene seals (spring loaded) enabled exposing of the gauge-section of the specimen to the selected test environment.

Test Media **:** The experiments were conducted to study the changes in mechanical properties and the mode(s) of failures in different concentrations of aqueous ammonia vis-à-vis an inert medium (air). Test solutions were prepared using double distilled water and LR grade 25% liquor ammonia. The pH Control was maintained through a 2.0-liter bulk solution. A constant flow of 60 ml/hr was provided under gravity through the corrosion chamber to maintain the pH level, and fresh bulk solution was introduced every 24 hours.

2.2 Testing and Raw Test Data

Individual specimens were mounted in the corrosion chamber and then subjected to an initial strain rate of $9.98^{*}\ 10^{-7}\ sec^{-1}$. The corresponding cross-head speed was 0.000576 cm/min. The ambient test temperature was 28° C ± 1° C. One sample was tested in air to verify the reproducibility with earlier tests[9,10,12]. Three samples each were tested in the selected concentrations of aqueous ammonia. The test results are summarized in Table 1. Fig.1 shows a plot of ammonia concentration v. average plastic strain ratio.

3. RESULTS AND ANALYSIS

3.1 Mechanical Strength Test Results

The air tested sample displayed the mechanical strength values similar to that observed in the earlier tests [9,10,12]. Both the load-bearing capacity (UTS) and the plastic strain ratio dropped steeply with ammonia concentrations upto 2.5%, and then changed gradually to become flat beyond ~7% ammonia, as indicated in Fig 1. The UTS dropped form 307.57 MNm^{-2} in the inert environment to 216.12 MNm^{-2} with 5% aqueous

ammonia, and then it changed gradually to 198.92 MNm^{-2} at 12.5% aqueous ammonia concentration. The deterioration in the load-bearing capacity of the alloy with increasing concentrations of ammonia was clearly evident from the results. Even though the failures at all ammonia concentrations had occurred beyond the elastic zone, the resulting failures were brittle in nature. The time to failure dropped from 75.5 hours in air to 52.01 hours in 12.5% ammonia.

3.2 Visual Examination and Optical Microscopy

Fig. 2 shows an optical view of the as-tested specimens. It clearly showed a systematic reduction in the specimen elongation, from the air-tested specimen to the specimens tested with increasing concentrations of ammonia, similar to the trend observed in Fig. 1. The observed surface corrosion and cracking became more severe with increasing ammonia concentrations, and the corresponding specimen fractures became more and more brittle (Figs. 3a and 4a).

Following this initial evaluation, one half of each fractured sample was ultrasonically cleaned in a mild ALCANOX solution to remove the surface corrosion products. The cleaned samples (Figs. 3b, 4b and 5) were then examined under a stereo-optical microscope.

The air tested specimen showed a completely ductile fracture. The 1% ammonia specimen did not exhibit surface cracks, but a non-ductile fracture was visually evident. The specimens tested at 2.5% and higher ammonia concentrations showed distinct surface SCC and increasingly brittle fractures. The failure in the 12.5% ammonia sample was completely brittle and displayed a very high density of surface cracks. Fig. 5 shows a cross-sectional views of the specimens. It confirmed a brittle and rough fracture that had originated from multiple surface (SCC) cracks in higher concentrations of ammonia.

3.3 Analysis of the Corrosion Products

The corrosion products observed on the fractured surface of the specimen tested in air was mainly copper oxide(s). The specimens tested in various concentrations of aqueous ammonia all showed similar EDX spectra from the corrosion products (Fig. 6). The low observed amounts of Ni, Mn and Fe in the corrosion products indicated that the copper was being preferentially attacked. Some dissolution of these elements in the running test solution is also possible.

All the aqueous ammonia tested specimens exhibited crystalline corrosion products. Fine crystalline corrosion products were observed at low ammonia concentrations (Figs 7a and 7b). Then, with increasing ammonia concentrations, the corrosion product crystal size increased (matured) for up to 5% ammonia and then the size remained essentially unchanged at higher ammonia concentrations (Figs. 7c, 7d and 7e).

The present corrosion product analyses suggested that the corrosion products that are formed upon aqueous ammonia exposure are mainly copper oxides. However, the EDX

technique does not detect hydrogen. Therefore, the presence of some copper hydroxides in the present corrosion products cannot be completely ruled out.

3.4 Determination of Crack Depths and Corrosion Penetration

The uncleaned halves of the failed samples were cut at ~ 1.0 in. from the fractured end, longitudinally sliced in the middle of the sample width, then mounted in bakelite with the sliced thickness face down, and polished to a 0.05-micron surface finish. The polished X-sections were examined under SEM to study the depth penetration of the corrosion attack and the surface SCC cracks, and to characterize the operative fracture initiation and propagation mechanism(s) in the present failed samples.
The polished air-tested specimen had failed in a completely ductile mode with significant plastic deformation. This observation was consistent with the earlier test results [9,10,12]. No cracking and/or corrosion was involved in this failure.

Figures 8a-b show low magnification cross-sectional SEM views from the polished cross-sections from 1% to 12.5 % ammonia-tested samples. With increasing ammonia concentration, the fractures became increasingly brittle and the depth penetration of the SCC cracks also increased significantly. The 1% ammonia sample did not show any cracks, but a 26-micron thick general surface corrosion layer was observed in this sample. The sample tested in 1% ammonia appeared to have failed in a ductile mode (Fig. 8a top). However, some influence of other possible failure mechanisms could not be ruled out at this early stage.

The maximum SCC crack penetrations observed in 2.5, 5.0, 10.0 and 12.5 % ammonia samples were 89, 134, 211 and 401 microns, respectively. The SCC cracks had initiated at both the top and the bottom, surfaces in these samples. Increasing crack/corrosion penetration with increasing ammonia was a clear indication that SCC was the operative failure mode in these samples.

Typical cracks observed in the present polished samples were also examined at higher magnifications under the SEM to characterize the crack initiation and propagation mechanisms (Figs. 9a-b).

No cracks were observed in the 1% ammonia sample. The 2.5% ammonia sample showed zagged cracks, which are indicative of an intergranular corrosion attack, in the near-surface regions. The crack initiation regions of the 2.5 to 12.5 % ammonia samples had been obliterated by a severe corrosion. The crack propagation in the 2.5% and higher ammonia concentration tested samples had occurred by a transgranular SCC mechanism. The observed branching at the tip of the cracks in the 5% ammonia sample confirmed the presence of transgranular SCC. The SCC cracks in the 10.0 and 12.5% ammonia samples were severely corroded and, therefore, did not show the finer fracture features generally associated with the intergranular and transgranular SCC.

3.5 Examination of Polished and Etched Cross-sections from the Failed Samples

Figures 10 a-d shows the polished and etched cross-sections of the ammonia-tested samples. The 1% ammonia sample shows surface corrosion and no cracks (top photo in

Fig 10a), while 2.5% ammonia sample exhibited largely intergranular cracks (the lower SEM in Fig. 10a, which is from the bottom surface) confirming the SCC. The 5% ammonia tested sample (Fig 10b) clearly showed transgranular cracking even in small cracks (V-shaped). The 10% and 12.5% (Fig 10c,d)ammonia samples also exhibited transgranular cracks. The 12.5% ammonia sample displayed much thicker corrosion deposits on the surfaces as compared to other samples tested at the lower ammonia concentrations.

3.6 SEM Examination Of The Cleaned Fractures

The cleaned fractures from the air-tested and the ammonia-tested samples were examined in detail. The low-magnification overall views of the fractures and the representative magnified SEM views of the fracture initiation, propagation and the final failure regions from each failed sample were recorded and interpreted to obtain a better understanding of the operative failure modes and mechanisms in the present samples.

Figures 11 to 16 show composite low and high magnification SEM views obtained from the present failed samples that were tested in air and in 1% to 12.5% ammonia

The fracture in the air-tested sample (Fig.11) had originated in the middle-width region of the sample. The sample had failed essentially by a ductile dimple-rupture mode. Small shear lips were observed near the surfaces in the middle region. The presence of larger shear lips and overload fractures at the left and the right ends indicated that the fracture had propagated to both the left and right from the middle region. The right-hand end, where the shear lips were larger, is believed to have failed last. The air-tested specimen displayed significant thickness reduction and plastic deformation in the gage area before the final failure.

The polished X-section from the 1% ammonia-tested sample did not show any SCC (Fig. 12). However, some corrosion was observed on the fractured faces. The failure had originated in the middle interior (right middle, 200X SEM in Fig. 12) of the sample. The shear lips in this region were small and the fracture itself was more corroded because this area had failed first by a brittle corrosion attack. A typical brittle fracture was observed in the left upper middle portion of the fracture. The fracture progressed to the left and right from the middle region, accompanied by a significant plastic deformation of the sample. Both the left and the right ends showed a combination of ductile fracture with larger shear lips. The final overload fracture is believed to have occurred at the right end, which showed rougher, ductile dimple-rupture type fracture features and less corrosion. A similar failure was previously observed in samples tested in 3.5% NaCl + 10% $MgCl_2$ + 1% ammonia [9].

In the 2.5% ammonia-tested sample (Fig.13), the fracture originated from multiple intergranular SCC cracks from the bottom surface. The 60X view in Fig. 13 shows the brittle fracture at the left end. The fracture in this region started at the bottom by intergranular SCC, progressed by transgranular SCC and the top region failed by a ductile shear mode. The bottom middle, 400X SEM photomicrograph shows a magnified view of the intergranular SCC fracture
observed at the multiple initiation sites at the bottom surface.

The final fracture in the 2.5% ammonia sample occurred in the extreme right region, where the failure had started in an intergranular fashion at the bottom surface and progressed by a ductile shear mechanism (300X SEM in Fig. 13). The only corrosion observed in this region was in the initiation zone.
In the 5% ammonia-tested sample (Fig.14), the presence of severe corrosion tended to mask the evidence of the near-surface crack initiation mechanism(s), and the cracks appeared to be predominantly transgranular. This fracture initiated and progressed from multiple origins at both the surfaces to a significant depth. The observed fracture propagation appeared to be by a transgranular SCC mode. There was a narrow ductile region in the middle thickness region of the fracture. The left area (40X SEM in Fig. 14) showed a narrow ductile center region, which is believed to have failed first. The extreme right area ductile region (400X, right SEM in Fig. 14) was corroded and it may have failed before the middle right ductile region (final failure), which was not corroded (400 X, final fracture, middle SEM in Fig. 14).

The fracture in the 10% ammonia-tested sample (Fig.15) had originated at multiple locations on both the surfaces and progressed inwards by transgranular SCC to a significant depth of the sample thickness. The details of the fracture initiation sites had been obliterated by the corrosion attack. In the left region (40 X SEM, Fig. 15), the sample had fractured by a brittle SCC mode, through the entire thickness of the sample. Small, ductile fracture zones were observed in the center regions of the middle-right and the right-end areas of the fracture. The middle-right, ductile fracture was corroded and is believed to have failed before the uncorroded center ductile region at the extreme right in Fig. 15, which failed last under overload conditions (125 X SEM in Fig. 15).

The 12.5 % ammonia-tested sample fracture (Fig.16) had a brittle, smooth appearance through most of its thickness, probably due to a severe corrosion attack as a result of high ammonia concentration. This fracture started at multiple locations on both the surfaces and then rapidly progressed inwards by a transgranular SCC mechanism. The corrosion had completely obliterated the finer fracture features at the near-surface initiation sites. The left region of the fracture (40X SEM in Fig. 16) was brittle through the sample thickness and is believed to have failed first. The middle SEM photo at 250X in Fig. 16 shows a magnified view of the brittle SCC observed near the bottom surface in the middle-right area of the overall fracture. The right end of the overall fracture showed some corroded, ductile fracture (200X SEM in Fig. 16), and is believed to be the region of the final overload fracture in the present sample.

The present analytical work clearly showed that at all ammonia concentration levels, the initial SCC attack starts out at the outer sample surfaces essentially by an intergranular attack and then progresses by a transgranular SCC mechanism. In the samples tested at higher than 5% ammonia concentrations, the evidence of the initial near-surface, intergranular attack is quickly obliterated by the severe corrosion, which tends to dominate the failure process. The fracture propogation after the initial intergranular initiation essentially takes place by a transgranular SCC mode.

4. TIME SCALING OF CRACK PROPAGATION

The studies undertaken by the author on Cu-Ni specimen suggest that the ammonia concentration might be one of the key factors in determining the modes and mechanism of failures observed in Cu-Ni pipes in marine environments. Studies were carried out on Cu-5.37 %Ni alloy specimen in aqueous ammonia containing 1.0,2.5,5.0,10.0 and 12.5% ammonia. The deterioration in the load –bearing capacity of the alloy with increasing concentrations was clearly evident from the results (Table 2). The time to failure dropped from 75.5 hours in air to 52.01 in 12.5% ammonia.

It was also observed that with increasing ammonia concentrations , the fractures became increasingly brittle ,and the depth penetration of the stress –corrosion cracks increased significantly. Using the results of depth penetration and time to failure a relation ship between ammonia concentration and crack propagation rate can be generated (fig 10.).

It was observed that upto about 5 % of concentration of ammoniacal solution, the crack growth rate follows a linear relationship, beyond which there is exponential increase. The linear relationship range may be usefully utilized in predicting the failure time under low concentration of ammonia after accelerated lab testing at about 4 % ammonia concentration.

5.CONCLUSIONS

The results and observations obtained on a low-nickel copper alloy[14] indicated that the presence of ammonia generally initiates the SCC attack at sample surfaces by an intergranular mechanism. The subsequent fracture propagation occurs essentially by a transgranular SCC mechanism. The presence of ammonia modifies the failure modes and mechanisms in the present copper-nickel alloy, thereby compromising the load bearing capability and other mechanical properties. In low concentration region of ammonia, the crack propagation rate increases linearly with increase in concentration. With ammonia concentration greater than 5 %, the crack propagation increases exponentially.

Ammonia, irrespective of its concentration has been found to embrittle the Cu-Ni alloy. It has been demonstrated that the severity of the detrimental effects of ammonia generally become worse with prolonged exposure of the present alloy to ammonia [12]. A combination of the presence of service stresses in an engineering system, accompanied by localized release of unknown amounts of ammonia, can lead surface embrittlement and crack initiation by an intergranular corrosion mechanism. The dominant failure mechanism(s) after this initial surface embrittlement could be in the form of a mixed mode, which is invariably corrosion-assisted [9,10].

The present tested copper-nickel alloy has several possible applications in the marine environments. The bio-degradation of organism release varying rates of ammonia and the average concentration levels of ammonia in harbours can well be established. The rapid laboratory test suggested here, compared with the percentage of ammonia in natural conditions would provide a realistic time estimate of failure under SCC conditions.

6. ACKNOWLEDGMENTS

The author thanks Director IAT, Pune India, for extending the organisational support in the experimental work.

REFERENCES

[1] Alan Turnbull, 2002, Environmental Assisted Cracking, Conference Report, British Corrosion Journal , Vol 37, No. 2, pp 91
[2] Avner Sidney .H, 1974, Introduction to Physical Metallurgy, Chap.15, pp 583-604.
[3] Francis R., 1985, Effect of pollutants on Corrosion of Copper Alloys in sea water (Ammonia and Chlorine), British Corrosion Journal , Volume 20, No.4 pp 167
[4] Francis R., 1985, Effect of pollutants on Corrosion of Copper Alloys in sea water (Sulphide and Chlorine), British Corrosion Journal , Volume 20 No.4 page 175
[5] Harvey D.P., TS Sudarshan, MR Louthan,1988, Effect of pH on corrosion and monotonic loading behaviour of 90Cu-10Ni in 3.5% sodium chloride solution, British Corrosion Journal , Vol 23,No.1, pp 61
[6] Islam M., Riad W.T., AlKharaaz S., AboNamous S., 1991, Stress Corrosion Cracking Behavior of 90/10 Cu-Ni Alloy in Sodium Sulphide Solutions, Corrosion Journal, Vol 47, No. 4 , pp 260
[7] Jamal N Alhajji and Mahmoud R Reda, 1995, Effects of Sulphides on Corrosion of Cupro Nickel Alloys, J Electrochem Soc. Vol 142 No. 9
[8] Gilbert P.T.,1992, Corrosion Resisting Properties of 90/10 Copper-Nickel Iron Alloy with particular reference to Offshore Oil and Gas Applications, British Corrosion Journal , Vol 14, No. 1, pp 20
[9] Agarwal D.C., 2002, Effect of Ammonical sea water on material properties of Copper-nickel alloy", British Corrosion Journal , Vol 37, No. 2, pp 105
[10] Agarwal D.C., 2002, Stress Corrosion In Copper-Nickel Alloys – Influence Of Ammonia", accepted for British Corrosion Journal , Vol 37, No. 4.
[11] ISO 7539-7: 1989(E)
[12] Agarwal D.C. and Kurian S., 2002, Effect of harbour environment on copper nickel-alloy, International Seminar on Ship and Ocean Technology (SHOT-2002), IIT Kharagpur, India, 18 – 20 Dec 2002
[13] Standard E-8, ASTM, Philadelphia, PA 1992
[14] Agarwal D.C., 2003, Effect of Ammonia Concentration on Environment Assisted Failures of a Low-Nickel Copper Alloy", Practical Failure Analysis Journal , Vol 3(5).

Table 1

Environment	Expt. No.	Time to failure (Hours)	Max Stress (MN/sqm)	Elongation at guage length (mm)	Plastic Strain to failure (50mm guage length)	Average Plastic Strain ratio
AIR	1	75.54	307.57	16.96	0.339	1.0000
1 % NH3 (pH = 12.06]	AVG	62.93	277.40	14.50	0.290	0.8555
2.5 % NH3 (pH = 12.35)	AVG	61.88	237.86	14.26	0.285	0.8411
5 % NH3 (pH = 12.38)	AVG	57.26	216.12	13.19	0.264	0.7784
10 % NH3 (pH = 12.42)	AVG	52.14	205.71	12.01	0.240	0.7088
12.5 % NH3 (pH = 12.48)	AVG	52.01	198.92	11.98	0.240	0.7070

* all reading at the initial strain rate of $9.98*10^{-7}$ sec^{-1}

Table 2

Environment	Time to Failure	Max Stress,MN/m2	Depth penetration of stress corrosion cracks (μm)
Air	75.54	307.57	-
1% NH3 (pH=12.06)	62.93	277.86	NA
2.5% NH3 (pH=12.35)	61.88	237.86	89
5% NH3 (pH=12.38)	57.26	216.12	134
10% NH3 (pH=12.42)	52.14	205.71	211
12.5% NH3 (pH=12.48)	52.01	198.92	401

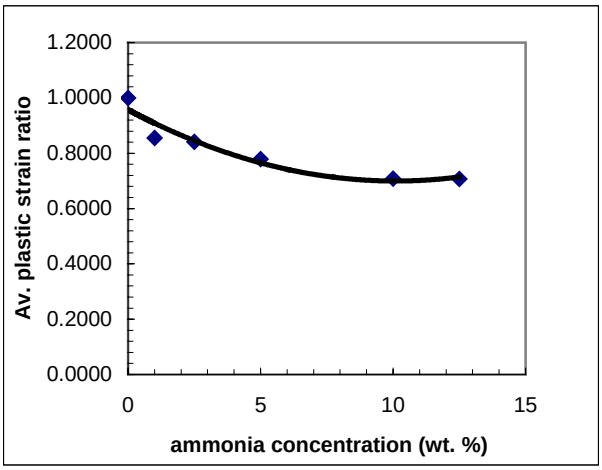

Fig. 1 Ammonia concentration to average plastic strain ratio

Fig 2 Tested samples

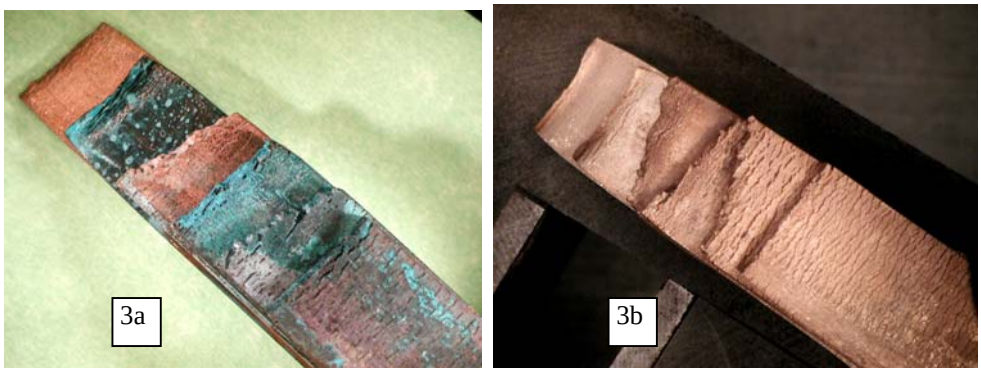

Fig 3 Surface cracks in (L to R) air & 1% to 12.5% ammonia (a) as tested (b) after cleaning

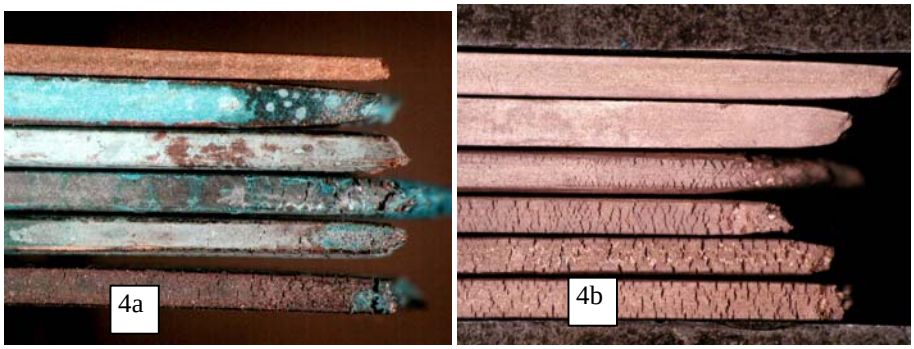

Fig 4 Side view cracks (top to bottom)air & 1% to 12.5% ammonia (a) as tested (b) Cleaned

Fig 5 X-section view, air & 1% to 12.5% ammonia

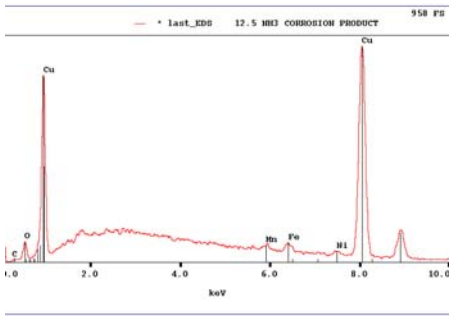

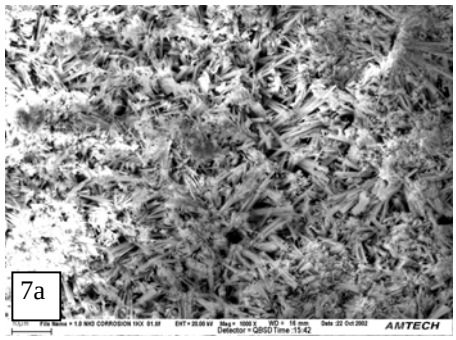

Fig 6 EDX of Corr. Products in ammonia

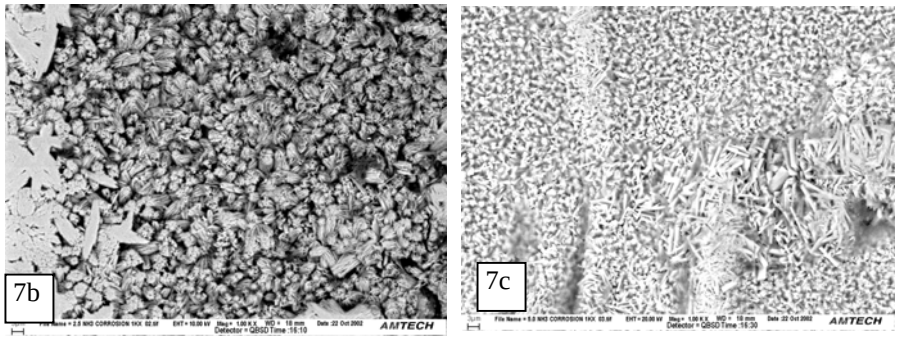

Fig 7 SEM of Corrosion Products (a) 1% (b) 2.5% (c) 5% ammonia

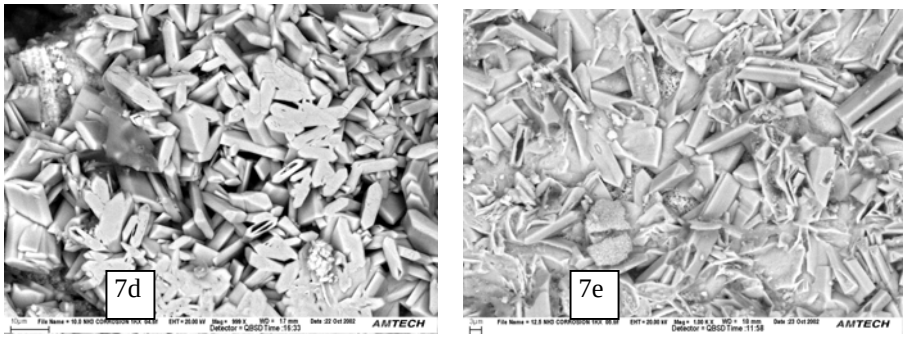

Fig 7 SEM of Corrosion Products (d) 10% (e) 12.5% ammonia

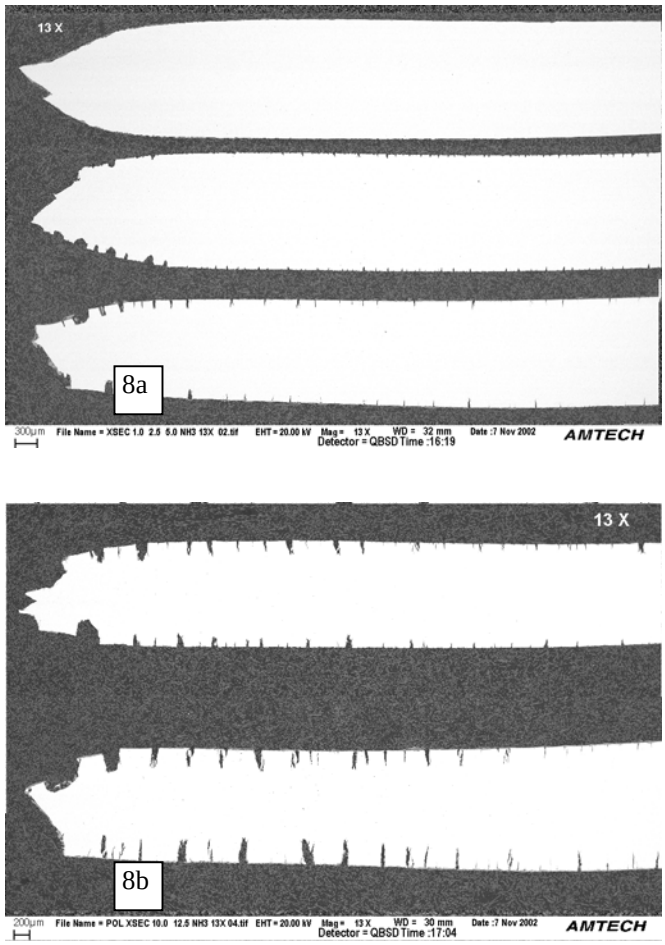

Fig 8 Polished x-sec 13X (a) 1%, 2.5%, 5% (b) 10%, 12.5% ammonia

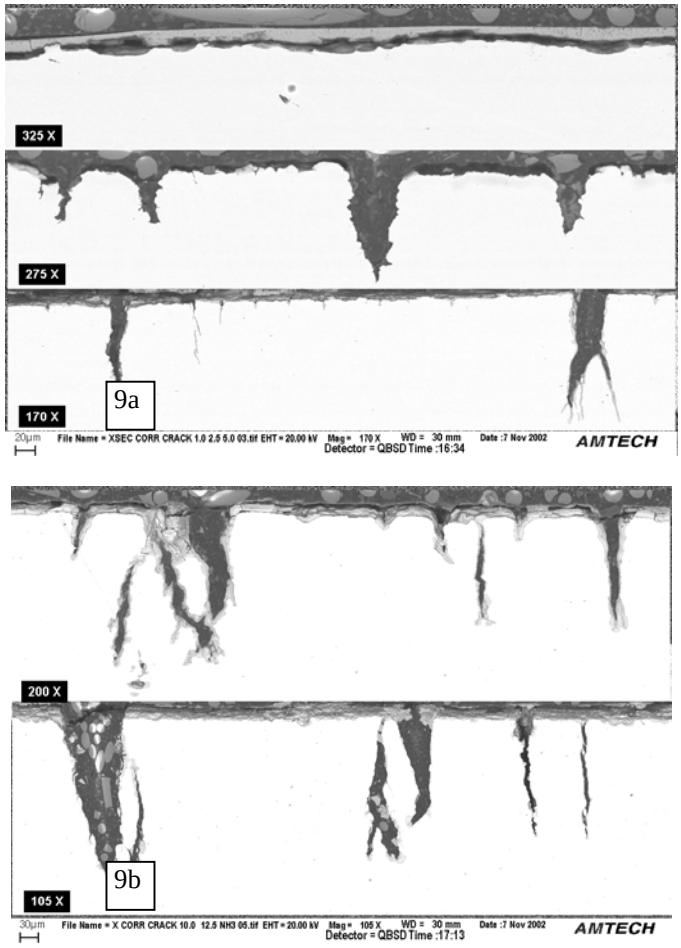

Fig 9 SEM -cracks un etched (a) 1%, 2.5%,5% (b) 10%, 12.5% ammonia

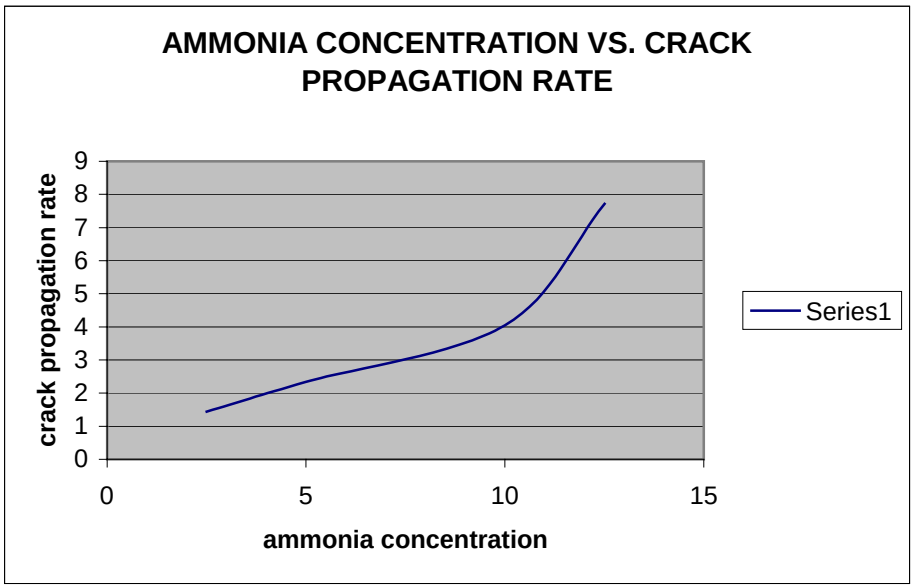

Fig. 10 shows relation ship between ammonia concentration and crack propagation rate

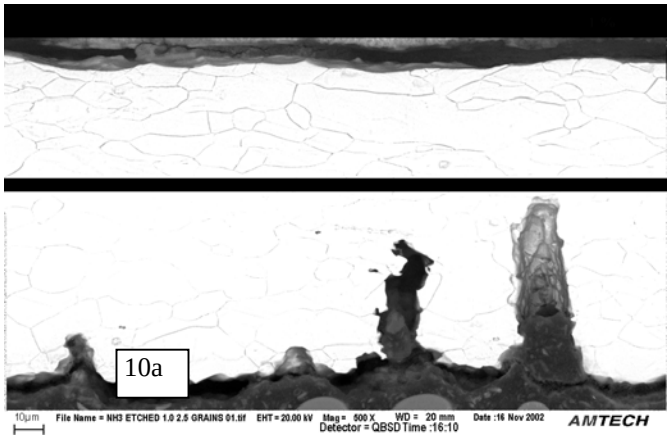
10a
10µm File Name = NH3 ETCHED 1.0 2.5 GRAINS 01.tif EHT = 20.00 kV Mag = 500 X WD = 20 mm Date :16 Nov 2002
Detector = QBSD Time :16:10
AMTECH

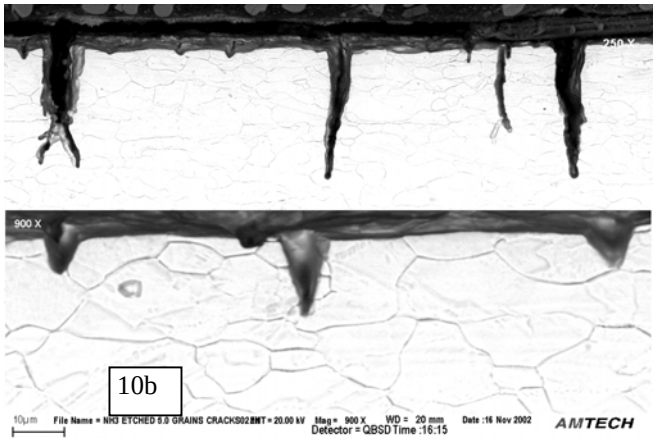
900 X
10b
10µm File Name = NH3 ETCHED 5.0 GRAINS CRACKS02 EHT = 20.00 kV Mag = 900 X WD = 20 mm Date :16 Nov 2002
Detector = QBSD Time :16:15
AMTECH

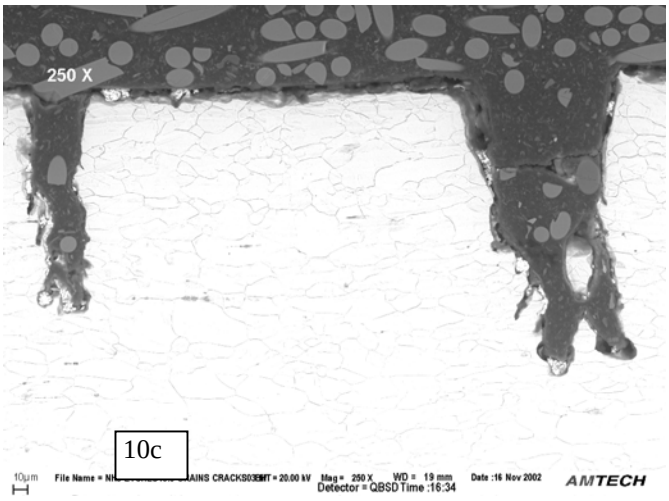
250 X
10c
10µm File Name = NH EHT = 20.00 kV Mag = 250 X WD = 19 mm Date :16 Nov 2002
Detector = QBSD Time :16:34
AMTECH

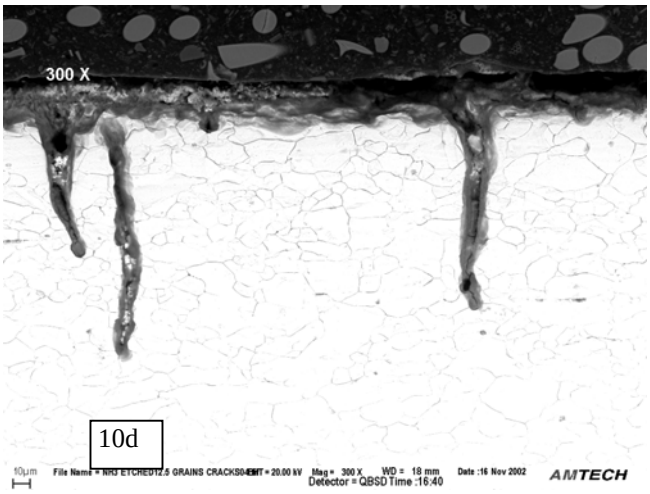

Fig 10 SEM of etched (a)1%, 2.5% ammonia (b) 5% ammonia (c) 10% ammonia (d) 12.5%
ammonia

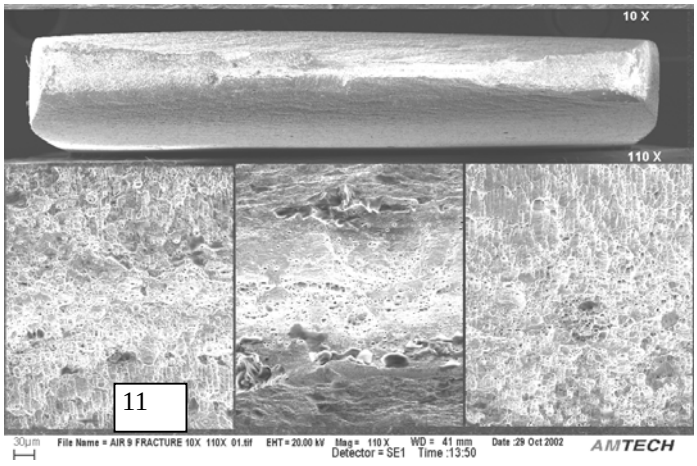

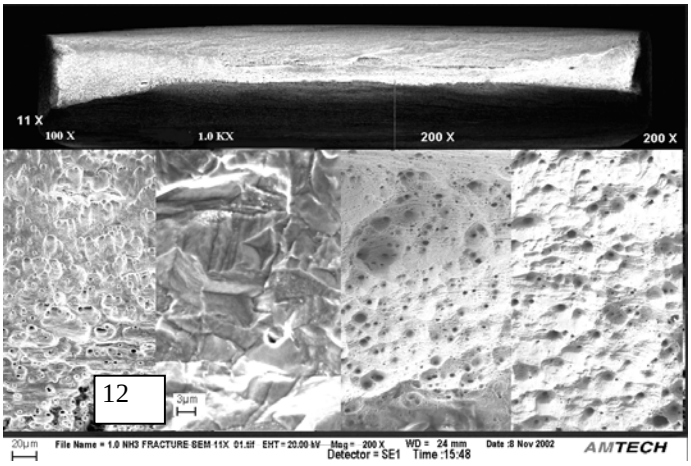

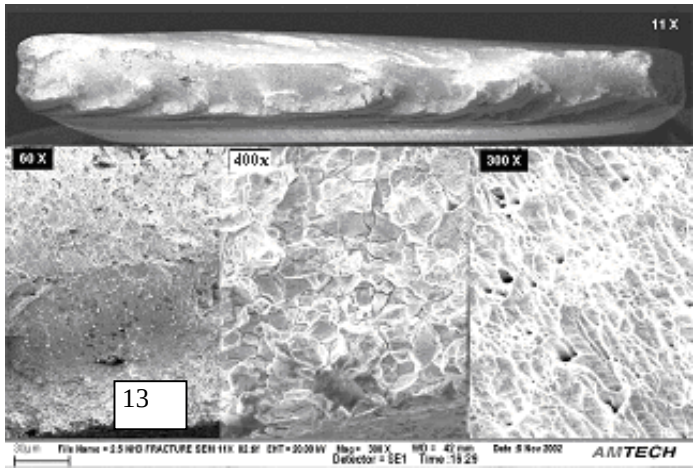
11 X
60 X
400x
300 X
13
AMTECH

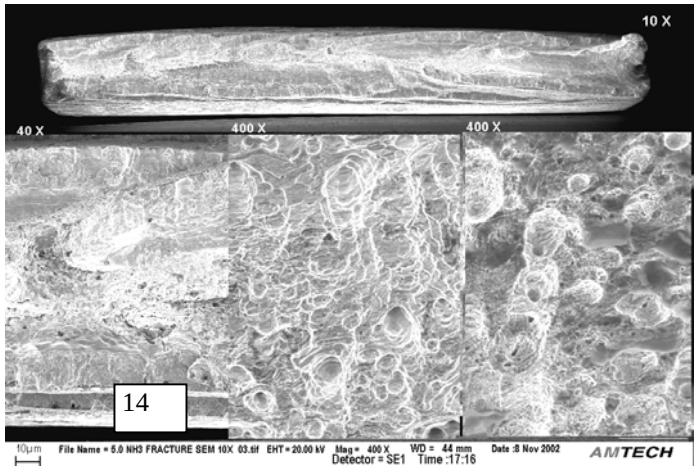
10 X
40 X
400 X
400 X
14
AMTECH

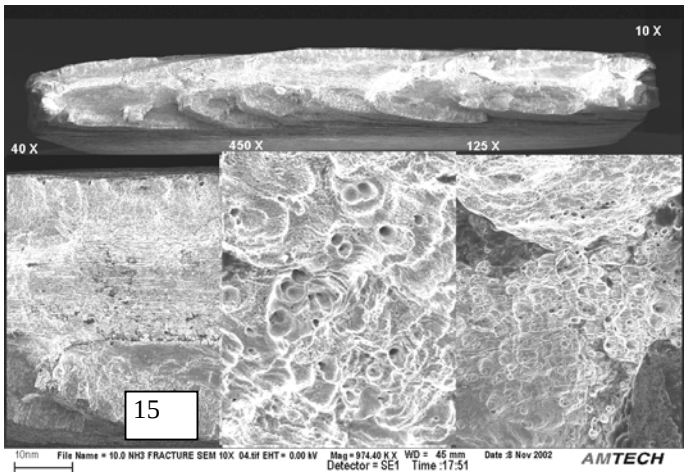
10 X
40 X
450 X
125 X
15
AMTECH

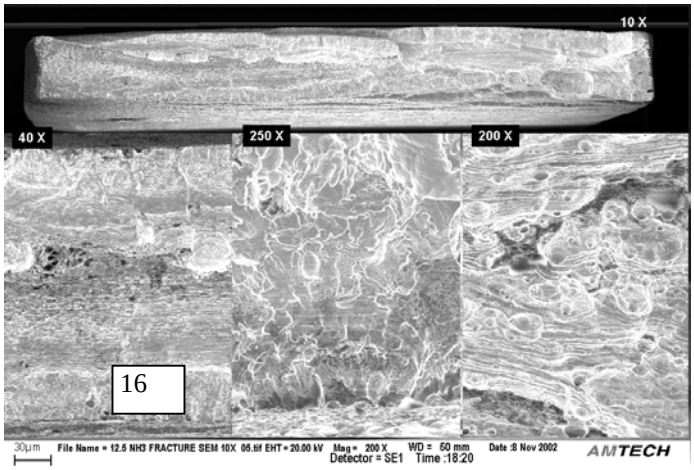

Composite SEM s: Fig 11- air; Fig 12– 1% ammonia; Fig 13– 2.5% ammonia; Fig 14– 5% ammonia; Fig 15– 10% ammonia; Fig 16– 12.5% ammonia